LETTER

Raman spectroscopic study of olivine-group minerals

Takashi MOURI and Masaki ENAMI

Department of Earth and Planetary Sciences, Nagoya University,
Chikusa-ku, Nagoya 464-8601, Japan

Synthetic end-members Mg_2SiO_4, Fe_2SiO_4, Mn_2SiO_4, and Co_2SiO_4 and natural samples of forsterite-fayalite series, tephroite and monticellite, are investigated using Raman spectroscopy. The Raman spectra of the olivine-group minerals have a characteristic set of two intense lines of the Si-O asymmetric stretching band (wavenumber κ_1) and Si-O symmetric stretching band (κ_2). The κ_1 and κ_2 values of the Mg_2SiO_4-Ca(Mg, Fe)SiO_4 series, in which the M2 site is occupied by nontransition elements, vary from 847 cm^{-1} to 857 cm^{-1} and from 815 cm^{-1} to 825 cm^{-1}, respectively, and their ω (= $\kappa_1 - \kappa_2$) value is fairly constant around 32 cm^{-1}. On the other hand, fayalite, tephroite, and other olivine-group minerals in which transition elements exist in the M2 site have a fairly constant κ_1 (836-839 cm^{-1}) value and variable κ_2 (808-819 cm^{-1}) and ω (20-32 cm^{-1}) values. The ω value of the forsterite-fayalite series systematically increases with Mg#[= Mg/(Mg + Fe)] and is useful for determining their chemical compositions.

Keywords: Chemical composition, Solid solution, Olivine, Raman spectra

INTRODUCTION

Laser Raman microspectroscopy is a powerful tool for the detection of minute inclusions in optically transmissive host phases. Therefore, it can be used for the following purposes: (1) identification of high- and ultrahigh-pressure phases present in diamond, zircon, and other container phases (e.g., Sobolev and Shatsky, 1990; Sobolev et al., 1995; Tabata et al., 1998; Gillet et al., 2002), (2) estimation of chemical compositions of fluid inclusions (Burke, 2001), and (3) measurement of residual pressures retained by solid and fluid inclusions (Sobolev et al., 2000; Yamamoto et al., 2002; Enami et al., 2007).

The Raman spectra of solid solution phases systematically shift depending on their chemical compositions and pressure and temperature conditions. Thus, laser Raman microspectroscopy is also useful in the determination of the chemical compositions of minute phases in terrestrial and extraterrestrial materials and inclusions in diamond and other phases (e.g., Wang et al., 2004). The relationships between chemical compositions and Raman frequency shifts of the forsterite-fayalite series – the common constituent of mantle materials and meteorites – have been calibrated by Wang et al. (2004) and Kuebler et al. (2006), and a large inconsistency have been found between them.

The objectives of the present study are (1) to report the characteristics of the Raman spectra of olivine end-members and (2) to newly calibrate the composition dependence of the Raman spectra of the forsterite-fayalite series.

EXPERIMENTAL DETAILS

Well-characterized synthetic single crystals of end-members Mg_2SiO_4, Fe_2SiO_4, Mn_2SiO_4, and Co_2SiO_4 (Sumino et al., 1977; Sumino, 1979) and natural samples of the forsterite-fayalite series, tephroite and monticellite, were used for Raman analyses. The chemical compositions of the natural olivine grains were determined using an electron-probe microanalyzer JEOL JXA-8800R (WDS + EDS). During the quantitative analyses, the accelerating voltage and specimen current of the Faraday cup were 15 kV and 12 nA, respectively (Table 1).

Raman spectra were obtained using a laser Raman microspectrophotometer Nicolet Almega XR (Thermo Fisher Scientific; gratings: 2400 lines/mm) equipped with a 532-nm Nd:YAG laser, a charge coupled device (CCD) detector (Andro Technology; 256 × 1024 pixels, cooled by a Peltier element), and an automated confocal microscope Olympus BX51. The objective lens was an Olympus Mplan-BD 100X lens (NA = 0.9). The room temperature was maintained at 22 ± 1 °C. Details of analytical precision have been discussed by Enami et al. (2007).

Table 1. Chemical compositions and localities of olivine for the Raman analyses

Mineral	Sample No.	Fe	Mn	Mg	Ca	Ni	Host rock	Locality
Fo-Fa	GO12Y06b	0.127	0.002	1.866	0.000	0.006	Peridotite	Sanbagawa belt/Besshi, Ehime
Fo-Fa	FR05	0.136	0.007	1.850	0.000	0.008	Dunite	Sanbagawa belt/Fujiwara, Ehime
Fo-Fa	KS71091517	0.153	0.002	1.836	0.000	0.009	Peridotite	Samburu, Kenya
Fo-Fa	OL02-g1	0.157	0.002	1.833	0.000	0.008	Peridotite	Unknown
Fo-Fa	OL01-g2	0.161	0.000	1.837	0.000	0.003	Peridotite	North Carolina, USA
Fo-Fa	OL01-g3	0.187	0.000	1.811	0.000	0.003	Peridotite	Unknown
Fo-Fa	OL02-g3	0.203	0.003	1.785	0.002	0.007	Peridotite	Unknown
Fo-Fa	OL02-g2	0.204	0.003	1.785	0.001	0.007	Peridotite	Unknown
Fo-Fa	HG04A01b (C)	0.300	0.005	1.688	0.003	0.004	Basalt	Abu/Hagi, Yamaguchi
Fo-Fa	HG04A01b (M)	0.465	0.009	1.519	0.005	0.002	Basalt	Abu/Hagi, Yamaguchi
Fo-Fa	HG04A01b (R)	0.568	0.013	1.410	0.006	0.003	Basalt	Abu/Hagi, Yamaguchi
Fo-Fa	HG04A02	0.704	0.010	1.275	0.007	0.005	Andesite	Abu/Hagi, Yamaguchi
Fo-Fa	TH83072308	0.793	0.011	1.195	0.001	0.000	Ol-gabbro	Ryoke belt/Kajishima, Ehime
Fo-Fa	GSJM17032	1.565	0.083	0.351	0.001	0.000	Dacite	Hakone/Yugawara, Kanagawa
Fo-Fa	99-01	1.635	0.046	0.306	0.012	0.000	Dacite	Mt. Kenami/Abukuma, Fukushima
Fo-Fa	99-02	1.657	0.047	0.282	0.013	0.000	Dacite	Mt. Kenami/Abukuma, Fukushima
Fo-Fa	OL01-g4	1.661	0.332	0.006	0.001	0.000	Pegmatite	Kawamata, Fukushima
Fo-Fa	GSJM16253	1.759	0.137	0.101	0.004	0.000	Pegmatite	Ugakei, Mie
Fo-Fa	7232915 (G01)	1.770	0.073	0.128	0.028	0.000	Trachyte	Oki-Dogo, Shimane
Fo-Fa	7232915 (G02)	1.861	0.082	0.030	0.028	0.000	Trachyte	Oki-Dogo, Shimane
Fo-Fa	KO83090411	1.871	0.099	0.029	0.001	0.000	Qtz-diorite	Ryoke belt/Anan, Nagano
Monticellite	MX107	0.069	0.007	0.916	1.008	0.000	Marble	California, USA
Monticellite	TN01	0.302	0.067	0.627	1.004	0.000	Marble	Kurio, Nagano
Tephroite	MU406	0.021	1.696	0.261	0.023	0.000	Mn-ore	Hokkejino, Kyoto
Tephroite	NC01	0.030	1.856	0.109	0.005	0.000	Mn-ore	Fujii mine/Mikata Fukui

Proportions of divalent cations are calculated as Fe + Mn + Mg + Ca + Ni = 2.0.
Abbreviations are: Fo-Fa, forsterite–fayalite series; C, core: M, mantle; R, rim; Ol–gabbro, olivine–gabbro; Qtz–diorite, quartz–diorite.

SPECTROSCOPIC RESULT

Major end-members

The factor group analysis predicts that the olivine structure with the *Pnma* symmetry has 36 Raman–active vibration modes: $11A_g + 11B_{1g} + 7B_{2g} + 7B_{3g}$ (Chopelas, 1991). The Raman spectra of the olivine crystals have a characteristic set of two intense lines near 858–837 cm^{-1} [κ_1: Si–O asymmetric stretching band A_g(Si–O)$_{a-str}$] and 825–808 cm^{-1} [κ_2: Si–O symmetric stretching band A_g(Si–O)$_{s-str}$] (Fig. 1), and their positions are determined by curve fitting using a Voigt function. These frequency shifts are well consistent with those reported in the literature (e.g., Chopelas, 1991; Pilati et al., 1995; Lin, 2001). A study of the range of κ_1 and κ_2 values and their differences, ω (κ_1–κ_2), for differing types of olivine group minerals using both data reported in this contribution and values from the literature for Ni-olivine and kirschsteinite reveals two distinct trends related to different compositional types. The first trend is represented by forsterite,

monticellite, and kirschsteinite; absolute values of κ_1 (858–847 cm^{-1}) and κ_2 (825–815 cm^{-1}) decrease in this order, but their ω values are approximately constant, around 32 cm^{-1}. The second trend is shown by the Ni-olivine, fayalite, Co-olivine, and tephroite series that displays decreasing κ_2 values (819–808 cm^{-1}) in this order, but approximately constant κ_1 values (837–839 cm^{-1}), which results in an increase in the corresponding ω values. A significant difference between the two trends is the type of dominant element occupying the large octahedral M2 site: for all members of the second trend this element belongs to the transition element series, whereas none of the first series minerals contain significant amounts of transition elements. There have been extensive discussions on whether the two intense frequencies κ_1 and κ_2 depend on (1) the volume of the M1 site (Piriou and McMillan, 1983), (2) the distortion of the SiO$_4$ tetrahedra in response to Ca substitution at the M2 site (Lam et al., 1990), and (3) the average mass (M) at the octahedral M1 and M2 sites, denoted by the parameter M$^{-0.5}$ (Chopelas, 1991). However, it is clear from Figure 2 that the relationships
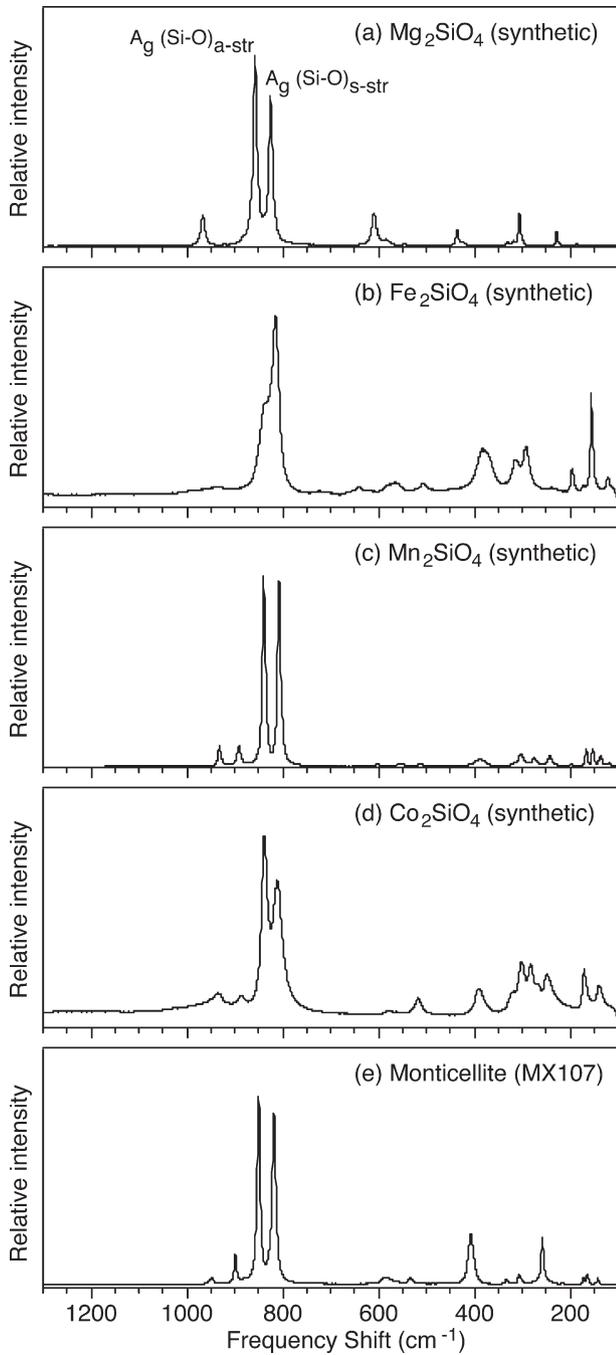
Figure 1. Ambient Raman spectra of olivine-group minerals.

Figure 2. κ_1, κ_2, and ω variations of olivine-group minerals. The abbreviations used are as follows: V denotes the unit-cell volume and C, the mass parameter ($M^{-0.5}$) proposed by Chopelas (1991). The Raman spectrum data are obtained from RRUFF database (http://rruff.info/) and Lin (2001). The unit-cell volume data are obtained from Sumino et al. (1976), Sumino (1979), Lin (2001), and RRUFF database.

Figure 3. Relationships between peak positions of the strongest doublet (κ_1 and κ_2) and Mg# value of forsterite-fayalite series.

between the frequency shifts and crystal chemistries of olivine are difficult to explain using only one of the proposed factors; for example, (1) the $CaMg_{-1}$ and $CaFe_{-1}$ substitutions at the M2 site affect the κ_1, κ_2, and ω values differently and (2) both the unit-cell volume and mass parameter $M^{-0.5}$ do not correlate well with the variations in the frequency shifts. These facts imply that the frequency shifts depend on other factors and/or coupling effects of the proposed factors. The systematic differences in the frequency shifts between the forsterite/monticellite/
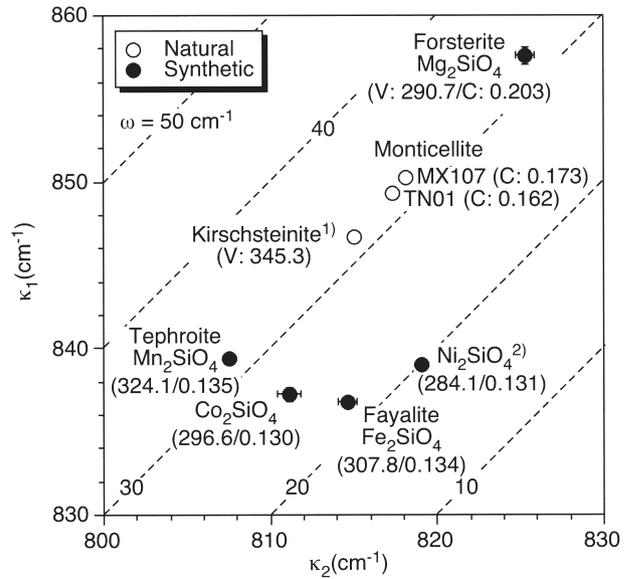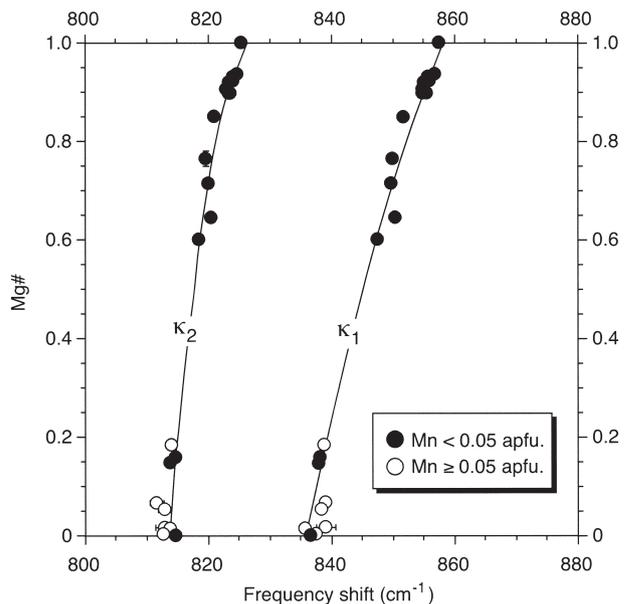
kirschsteinite series and the Ni-olivine/fayalite/Co-olivine/tephroite series possibly suggest that the behavior of the transition and nontransition elements at the M2 site is the main factor responsible of controlling the Raman spectra of olivine.
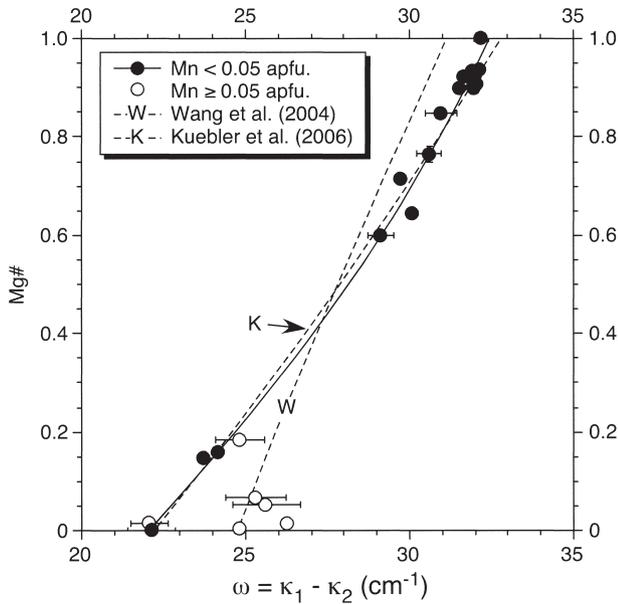
Figure 4. Relationships between ω and Mg# values of forsterite–fayalite series.

Forsterite-fayalite series

The relationships between the Mg#[= Mg/(Mg + Fe^{2+})] value and the Raman frequency shifts of olivine have been discussed by Guyot et al. (1986), Wang et al. (2004), and Kuebler et al. (2006). The data show positive correlations between the peak positions of the strongest doublet (κ_1 and κ_2) and the Mg# value of Mg-Fe olivine, although they exhibit slightly large scattering. We have recalibrated the relationships between the peak positions (κ_1 and κ_2) and the Mg# value of the olivine spectra (Fig. 3). The natural Fe-rich olivine generally contains considerable amounts of the tephroite component. The Mn content of Fe-rich olivine in this study is ~ 0.3 atoms per formula unit (apfu) for O = 4 (Table 1). Tephroite ($\kappa_1 = 839.3 \pm 0.1$ cm^{-1} and $\kappa_2 = 807.5 \pm 0.1$ cm^{-1}) has a higher κ_1 value and a lower κ_2 value than fayalite ($\kappa_1 = 836.8 \pm 0.5$ cm^{-1} and $\kappa_2 = 814.7 \pm 0.3$ cm^{-1}), and its incorporation into Fe-rich olivine increases the κ_1 value and decreases the κ_2 value. Our new calibrations of the κ_1-Mg# and κ_2-Mg# relationships obtained using the Mn-poor Mg-Fe olivine (Mn < 0.05 apfu) are as follows:

$$Mg\# = -610.65 + 1.3981\, \kappa_1 - 0.00079869\, \kappa_1^2$$
(correlation coefficient: $r^2 = 0.99$)

$$Mg\# = -3715.8 + 8.9889\, \kappa_2 - 0.0054348\, \kappa_2^2$$
($r^2 = 0.96$).

It would be preferable to use the difference between the ω values in order to avoid systematic errors in the

measurements of individual κ_i values and propose a new calibration technique for the frequency shift and Mg# value of olivine (Fig. 4). The ω value systematically increases with the Mg# value, except for limited Fe-rich olivines with Mg# < 0.2. The incorporation of the tephroite ($\omega = 31.8$ cm^{-1}) component into Fe-rich olivine (fayalite: 22.1 cm^{-1}) increases the ω value. Thus, the scattered ω values of Fe-rich olivine can be primarily attributed to the MnFe$_{-1}$ substitution. The calibrated ω-Mg# relationship is as follows:

$$Mg\# = -0.17744 - 0.050049\, \omega + 0.0026479\, \omega^2$$
($r^2 = 0.99$).

Our calibration is well consistent with the ω-Mg# relationship calculated from the dataset of Kuebler et al. (2006). The measurement precision of ω is 0.4 cm^{-1} or less in the conventional Raman analysis and results in an accuracy of 0.03-0.04 in the determination of Mg#.

Application and discussion

Raman spectroscopy is advantageous for the estimation of chemical compositions of solid solution phases present in optically transmissive host phases such as diamond. The inclusions, however, retain compressive or tensile stresses (e.g., Sobolev et al., 2000; Enami et al., 2007), and the measured frequency shifts of solid solution phases integrate the information on their chemical compositions and internal stress. The values of the pressure derivatives (dκ_i/dP) of the κ_1 and κ_2 values of forsterite are 2.85-3.27 cm^{-1} GPa^{-1} and 3.07-3.12 cm^{-1} GPa^{-1}, respectively (Chopelas, 1990; Wang et al., 1993). On the other hand, the values of the pressure dependence of ω are in the range of -0.22-0.15 cm^{-1} GPa^{-1}, which are one order of magnitude less than those of κ_1 and κ_2 values.

Izraeli et al. (1999) have estimated the residual pressure retained in the olivine inclusions in diamond to be 0.13-0.65 GPa based on their frequency shift (κ_1) relative to a free olivine grain (0.4-2.0 cm^{-1}) and calculated the mantle residual pressures to be 4.4-5.2 GPa at 1200 °C. In their calculation, the olivine composition is assumed to be independent of Mg# = 0.93. However, our calibration indicates that the measured frequency shifts (κ_1: 0.4-2.0 cm^{-1}) can be induced by the Mg# changes of 0.01-0.06, thereby eliminating the effect of the residual pressure. Although the olivine inclusions in diamond are fairly uniform in composition, the variations in their Mg# values of up to 0.04 (e.g., Tsai et al., 1979; Sobolev et al., 1997) are significant for the olivine Raman barometer. Thus, the postulated constant olivine composition (Mg# = 0.93; Izraeli et al., 1999) probably has significant effects on the

calculation of the residual and source pressures. The residual pressure of an olivine inclusion should be carefully estimated using combinations of κ_1/κ_2 values that are sensitive to pressure and composition and ω value that are sensitive to composition.

REFERENCES

Burke, E.A.J. (2001) Raman microspectrometry of fluid inclusions. Lithos, 55, 139-158.

Chopelas, A. (1990) Thermal properties of forsterite at mantle pressure derived from vibrational spectroscopy. Physics and Chemistry of Minerals, 17, 149-156.

Chopelas, A. (1991) Single crystal Raman spectra of forsterite, fayalite, and monticellite. American Mineralogist, 76, 1101-1109.

Enami, M., Nishiyama, T. and Mouri, T. (2007) Laser Raman microspectrometry of metamorphic quartz: A simple method for comparison of metamorphic pressures. American Mineralogist, 92, 1303-1315.

Gillet, P., Sautter, V., Harris, J., Reynard, B., Harte, B. and Kunz, M. (2002) Raman spectroscopic study of garnet inclusions in diamonds from the mantle transition zone. American Mineralogist, 87, 312-317.

Guyot, F., Boyer, H., Madon, M., Velde, B. and Poirier, J.P. (1986) Comparison of the Raman microprobe spectra of $(Mg,Fe)_2SiO_4$ and Mg_2GeO_4 with olivine and spinel structures. Physics and Chemistry of Minerals, 13, 91-95.

Izraeli, E.S., Harris, J.W. and Navon, O. (1999) Raman barometry of diamond formation. Earth and Planetary Science Letters, 173, 351-360.

Kuebler, K.E., Jolliff, B.L., Wang, A. and Haskin, L.A. (2006) Extracting olivine (Fo-Fa) compositions from Raman spectral peak positions. Geochimica et Cosmochimica Acta, 70, 6201-6222.

Lam, P.K., Yu, R., Lee, M.W. and Sharma, S.K. (1990) Sructural distortions and vabrational modes in Mg_2SiO_4. American Mineralogist, 75, 109-119.

Lin, C.C. (2001) High-pressure Raman spectroscopic study of Co- and Ni-olivines. Physics and Chemistry of Minerals, 28, 249-257.

Pilati, T., Demartin, F. and Gramaccioli, C.M. (1995) Thermal parameters for minerals of the olivine group: their implication of vibrational spectra, thermodynamic functions and transferable force fields. Acta Crystallographica, B51, 721-733.

Piriou, B. and McMillan, P. (1983) The high-frequency vibrational spectra of vitreous and crystalline orthosilicates. American Mineralogist, 68, 426-443.

Sobolev, N.V. and Shatsky, V.S. (1990) Diamond inclusions in garnets from metamorphic rocks; a new environment for diamond formation. Nature, 343, 742-746.

Sobolev, N.V., Shatsky, V.S., Vavilov, M.A. and Goryaynov, S.V. (1995) Zircon in high-pressure metamorphic rocks in folded regions as a unique container of inclusions of diamond, coesite, and coexisting minerals. Transactions of the Russian Academy of Sciences. Earth Science Sections, 336, 79-85.

Sobolev, N.V., Kaminsky, F.V., Griffin, W.L., Yefimova, E.S., Win, T.T., Ryan, C.G. and Botkunov, A.I. (1997) Mineral inclusions in diamonds from the Sputnik kimberlite pipe, Yakutia. Lithos, 39, 135-157.

Sobolev, N.V., Fursenko, B.A., Goryainov, S.V., Shu, J., Hemley, R.J., Mao, H.K. and Boyd, F.R. (2000) Fossilized high pressure from the Earth's deep interior: the coesite-in-diamond barometer. Proceedings of National Academy of Sciences, USA, 97, 11875-11879.

Sumino, Y. (1979) The elastic constants of Mn_2SiO_4, Fe_2SiO_4 and Co_2SiO_4, and the elastic properties of olivine group minerals at high temperature. Journal of Physics of Earth, 27, 209-238.

Sumino, Y., Ohno, I., Goto, T. and Kumazawa, M. (1976) Measurement of elastic constants and internal frictions on single-crystal MgO by rectangular parallelepiped resonance. Journal of Physics of Earth, 24, 263-273.

Sumino, Y., Nishizawa, O., Goto, T., Ohno, I. and Ozima, M. (1977) Temperature variation of elastic constants of single-crystal forsterite between −l90 degrees and 400 °C. Journal of Physics of Earth, 25, 377-392.

Tabata, H., Maruyama, S. and Shi, Z. (1998) Metamorphic zoning and thermal structure of the Dabie ultrahigh-pressure-high-pressure terrane, central China. The Island Arc, 7, 142-158.

Tsai, H.M., Meyer, H.O.A., Moreau, J. and Milledge, H.J. (1979) Mineral inclusions in diamond: Premir, Jagersfontein and finsh kimberlite, South Africa, and Williamson mine, Tanzania. In Kimberlites, Diatremes, and Diamonds: Their Geology, Petrology, and Geochemistry (Boyd, F.R. and Meyer, H.O.A. Eds.). 1, American Geophysical Union, Washington, D.C., 16-26.

Wang, A., Kuebler, K.E., Jolliff, B.L. and Haskin, L.A. (2004) Mineralogy of a Martian meteorite as determined by Raman spectroscopy. Journal of Raman Spectroscopy, 35, 504-514.

Wang, S.Y., Sharma, S.K. and Cooney, T.F. (1993) Micro-Raman and infrared spectral study of forsterite under high pressure. American Mineralogist, 78, 469-476.

Yamamoto, J., Kagi, H., Kaneoka, I., Lai, Y., Prikhod'ko, V.S. and Arai, S. (2002) Fossil pressures of fluid inclusions in mantle xenoliths exhibiting rheology of mantle minerals; implications for the geobarometry of mantle minerals using micro-Raman spectroscopy. Earth and Planetary Science Letters, 198, 511-519.